Journal of Electronics, Electromedical Engineering, and Medical Informatics
Homepage: jeeemi.org; Vol. 8, No. 4, October 2026, pp: 1702-1718 e-ISSN: 2656-8632

RESEARCH ARTICLE OPEN ACCESS

Subject-Level Aggregated Wavelet Packet Energy-Variance Features for EEG-Based Autism Spectrum Disorder Classification

Zaky Naufal[1], Melinda Melinda[1], Siti Rusdiana[2], Yunidar Yunidar[1], Aufa Rafiki[1], and Lola Vivita[3]

[1] Department of Electrical and Computer Engineering, Faculty of Engineering, Universitas Syiah Kuala, Banda Aceh, Indonesia
[2] Department of Mathematics, Faculty of Mathematics and Natural Sciences, Universitas Syiah Kuala, Banda Aceh, Indonesia
[3] Banda Aceh City Regional Development Planning Agency, Banda Aceh, Indonesia

Corresponding author: Melinda Melinda (e-mail: melinda@usk.ac.id), **Author(s) Email**: Zaky Naufal (e-mail: zaky.24@mhs.usk.ac.id), Siti Rusdiana (e-mail: siti.rusdiana@usk.ac.id), Yunidar Yunidar (e-mail: yunidar@usk.ac.id), Aufa Rafiki (e-mail: aufa35@mhs.usk.ac.id), Lola Vivita (e-mail: lolavivita@yahoo.com)

Abstract **This study addresses a key clinical challenge in EEG-based autism spectrum disorder (ASD) diagnosis: most prior work reports accuracy at the window level, whereas the clinical diagnostic unit is the individual subject, a mismatch that can inflate performance estimates. We develop and validate a subject-level EEG feature aggregation framework, combining Wavelet Packet Transform (WPT) energy-variance features, fold-safe ANOVA feature selection, and per-subject aggregation, evaluated under leakage-safe nested leave-one-subject-out (LOSO) cross-validation. Sixteen-channel EEG was recorded from 16 participants (8 ASD, 8 neurotypical) in Banda Aceh, Indonesia, using a single OpenBCI Cyton board with a Daisy module for native simultaneous 16-channel acquisition, preprocessed with Infomax ICA artifact removal, and classified using Logistic Regression. The framework achieved a nested LOSO balanced accuracy of 93.75% (F1 = 0.9412); because this estimate derives from only 16 subjects, the repeated subject-pair evaluation (balanced accuracy 0.9525 ± 0.0529, AUC 0.9897 ± 0.0163, permutation p = 0.0196) is treated as the primary robustness indicator. A learning-curve analysis indicated that performance approaches, but has not fully reached, a plateau at this cohort size. Sensitivity analyses across nine window/overlap configurations and six wavelets, selected within the nested cross-validation, confirmed the result was not selection-dependent. A controlled ablation indicated Infomax ICA outperformed MSICA-DWT (Wilcoxon p < 0.001), though a participant-level bootstrap interval was wide and included zero, reflecting the limited power of the 16-subject cohort. Overall, these results demonstrate the methodological feasibility of subject-level WPT energy-variance aggregation for leakage-safe ASD screening research rather than diagnostic readiness, and external multicenter validation on larger, demographically characterized cohorts is required before any clinical use.**

Keywords **Wavelet Packet Transform; Subject-level aggregation; Infomax ICA; LOSO cross-validation; Logistic Regression.**

I. Introduction

Autism Spectrum Disorder (ASD) is a neurodevelopmental condition characterized by persistent differences in social communication, restricted interests, and repetitive behavioral patterns. The global burden of ASD affects tens of millions of individuals and continues to rise, underscoring the clinical urgency of earlier and more scalable detection methods [1]. Behavioral assessment alone is time-consuming and dependent on clinician expertise, motivating the search for objective neurophysiological biomarkers that can complement diagnosis and support earlier, more scalable screening [2], [3]. Large-scale consortium efforts have been established specifically to validate candidate EEG biomarkers for clinical trial readiness in ASD [4].

Electroencephalography (EEG) has emerged as a promising objective biomarker for ASD because it is non-invasive, has high temporal resolution, and is sensitive to cortical activity patterns associated with neurodevelopmental differences; studies using EEG connectivity and source-level network analysis have consistently reported atypical functional and effective connectivity in children with ASD compared to

Manuscript received 6 July 2026; Revised 4 September 2026; Accepted 15 October 2026; Available online 29 October 2026
Digital Object Identifier (**DOI**): https://doi.org/10.35882/jeeemi.v8i4.1908
Copyright © 2026 by the authors. This work is an open-access article and licensed under a Creative Commons Attribution-ShareAlike 4.0 International License (CC BY-SA 4.0).

neurotypical peers [5], [6]. This potential has been broadly documented in review literature covering EEG-based ASD assessment and physiological biomarkers more generally [7], [8]. Beyond EEG alone, complementary multimodal approaches combining EEG with eye-tracking have also been proposed to identify diagnostic markers in ASD [9], [10]. Recent EEG-ASD classification studies have reported strong performance using classical machine learning on spectral and connectivity features [11], [12], [13], [14], deep learning architectures such as CNN-LSTM, transfer learning, graph convolutional networks, and time-frequency synergy networks [15], [16], [17], [18], and interpretable wavelet- and entropy-based feature engineering approaches [19]. A comparative review of such models and features further highlights the diagnostic utility of EEG-based machine learning across related neurodevelopmental conditions [20].

Despite these advances, many EEG-based ASD classification studies report performance at the window or segment level rather than at the individual subject level. This distinction is important because a single participant can contribute numerous correlated EEG windows. When windows from the same participant are included in both training and testing sets, data leakage may occur and lead to overly optimistic performance estimates [21], [22], [23], [24]. Subject-independent validation addresses this concern by separating participants between training and testing sets, integrating subject-level feature aggregation with a leakage-safe nested validation protocol, rather than introducing WPT, ICA, ANOVA, or Logistic Regression as new methods. Furthermore, deep learning approaches may face challenges related to training data requirements and model interpretability, particularly when applied to small, single-site EEG cohorts. Comparisons of single-stage ICA and multiscale denoising methods under a consistent subject-independent evaluation protocol also remain limited.

To address this gap, this study proposes a subject-level Wavelet Packet Transform (WPT) energy-variance aggregation framework for EEG-based ASD classification. Window-level WPT relative energy and variance features are extracted, fold-wise feature selection is performed strictly within the training fold, and the selected window-level features are aggregated into fixed-length per-subject representations using distributional statistics (mean, standard deviation, median, and interquartile range) prior to classification with Logistic Regression.

The aim of this study is to develop and rigorously validate a subject-level EEG feature aggregation framework that evaluates ASD classification performance at the individual level, using nested leave-one-subject-out (LOSO) cross-validation and repeated subject-pair validation to provide a leakage-safe,

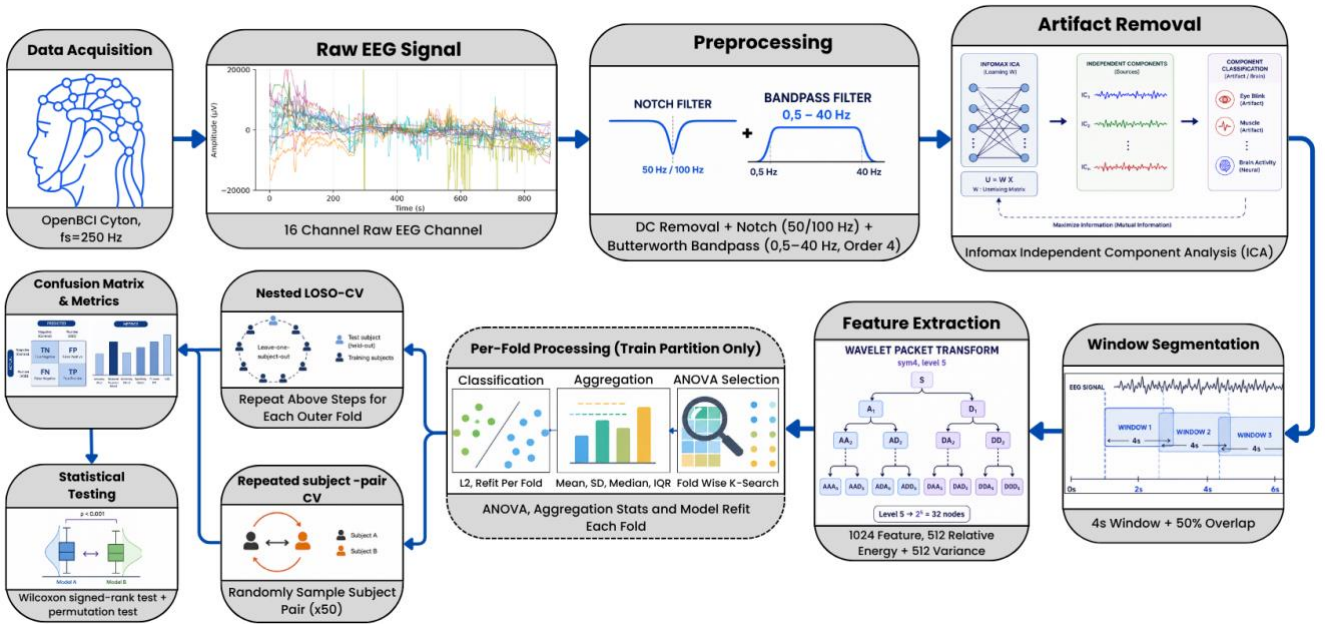

Fig. 1. Overall workflow of the proposed subject-level WPT energy-variance aggregation framework for EEG-based ASD classification.

providing a more appropriate assessment of classification performance on previously unseen subjects. Accordingly, the present study contributes by clinically meaningful performance estimate suitable for small cohorts. The main contributions of this study are as follows:

Manuscript received 6 July 2026; Revised 4 September 2026; Accepted 15 October 2026; Available online 29 October 2026
Digital Object Identifier (**DOI**): https://doi.org/10.35882/jeeemi.v8i4.1908
Copyright © 2026 by the authors. This work is an open-access article and licensed under a Creative Commons Attribution-ShareAlike 4.0 International License (CC BY-SA 4.0).

1) A fold-safe subject-level aggregation approach that transforms window-level WPT relative energy-variance features into per-subject statistical representations, aligning the evaluation unit with the clinical diagnostic unit.
2) A strict, leakage-safe evaluation strategy combining nested LOSO cross-validation, subject-pair validation, repeated subject-pair validation, and permutation testing to quantify robustness under a small-cohort setting.
3) A controlled ablation and statistical comparison (Wilcoxon signed-rank test) isolating the effect of Infomax ICA versus multiscale ICA-based denoising (MSICA-DWT) under an identical downstream WPT and Logistic Regression configuration.
4) A contextual benchmarking of the proposed framework against recent EEG-ASD classification studies, explicitly reporting differences in evaluation unit (subject-level versus window/segment-level) to support fair interpretation.

Wavelet-based methods are also widely used in EEG-ASD research; recent studies have applied wavelet packet decomposition, flexible analytic wavelet transforms, wavelet scattering, and discrete wavelet features for biomedical EEG classification [19], [25], [26], [27], [28]. The present study is also methodologically distinct from our group's previous work using overlapping data: A companion study using the same cohort compared MSPCA and MSICA under pooled window-level evaluation with LightGBM and TCN-SA classifiers [29]. In contrast, the present study evaluates classification at the subject level under a leakage-safe nested design rather than proposing new denoising algorithms or classifiers. Reference [30], which also draws on recordings from the same acquisition setup, instead optimizes Butterworth-PID preprocessing parameters via a Bayesian search, a preprocessing-tuning objective distinct from the subject-level aggregation and nested-LOSO evaluation framework developed here. In both cases, the shared element is the acquisition setup and participant pool; the genuinely new contribution here is the subject-level WPT energy-variance aggregation evaluated under leakage-safe nested LOSO.

The remainder of this paper is organized as follows. Section II describes the dataset, preprocessing pipeline, WPT feature extraction, subject-level aggregation strategy, classification model, and evaluation protocol. Section III presents the window-level and subject-level results, robustness validation, preprocessing ablation, and statistical comparison. Section IV discusses the interpretation, comparison with recent studies, and limitations. Section V concludes the paper.

II. Materials and Methods

This section presents the dataset, preprocessing pipeline, feature extraction approach, subject-level aggregation strategy, classification model, and evaluation protocol used in this study. The overall workflow is shown in Fig. 1.

A. Dataset

EEG recordings were collected at Universitas Syiah Kuala (USK), Banda Aceh, Indonesia, under ethics approval No. 117/EA/FK/2024. Consumer-grade EEG systems such as OpenBCI have been validated as viable platforms for research-grade EEG acquisition [31]. The dataset consisted of resting-state, eyes-open EEG signals acquired using a single OpenBCI Cyton board paired with a Daisy module, which provided native 16-channel simultaneous acquisition per participant at a sampling frequency of 250 Hz without requiring manual synchronization between separate boards. Electrodes were positioned according to the international 10-20 electrode placement system at Fp1, Fp2, F7, F3, F4, F8, T3, C3, C4, T4, T5, P3, P4, T6, O1, and O2 [30]. Recordings were monitored in real time using the OpenBCI GUI, and raw signals were saved in text format together with session notes and quality information [30]. EEG signal quality was controlled during acquisition by conducting recordings in a quiet, controlled room and checking electrode contact before each session; numerical electrode impedance values were not recorded by the OpenBCI system; signal quality was therefore instead assessed post hoc using objective indices computed from the raw recordings, including RMS amplitude, saturation/rail rate, flatline rate, 50 Hz line-noise ratio, and high-frequency noise. Of 256 channel-recordings (16 channels x 16 subjects), 210 were rated good, 23 marginal, and 23 poor; ASD-06 and ASD-04 showed elevated 50 Hz line-noise. Window rejection due to excessive amplitude (>500 uV peak-to-peak) averaged 1.74% of windows per subject (range 0.00-11.14%), with ASD-06 showing the highest rejection rate (11.1%). The cohort analyzed here reflects the dataset available at the time of this study; data collection within the research group is ongoing, and the participant pool is expected to grow in future work.

The final cohort consisted of 16 participants (8 ASD, 8 neurotypical controls). These 16 participants were selected from a larger pool of approximately 20 individuals recruited by the research group; because the original pool was imbalanced between ASD and neurotypical participants, a class-balanced subset of 8 participants per group was retained for the present analysis. Participants were recruited through voluntary,

Manuscript received 6 July 2026; Revised 4 September 2026; Accepted 15 October 2026; Available online 29 October 2026
Digital Object Identifier (**DOI**): https://doi.org/10.35882/jeeemi.v8i4.1908
Copyright © 2026 by the authors. This work is an open-access article and licensed under a Creative Commons Attribution-ShareAlike 4.0 International License (CC BY-SA 4.0).

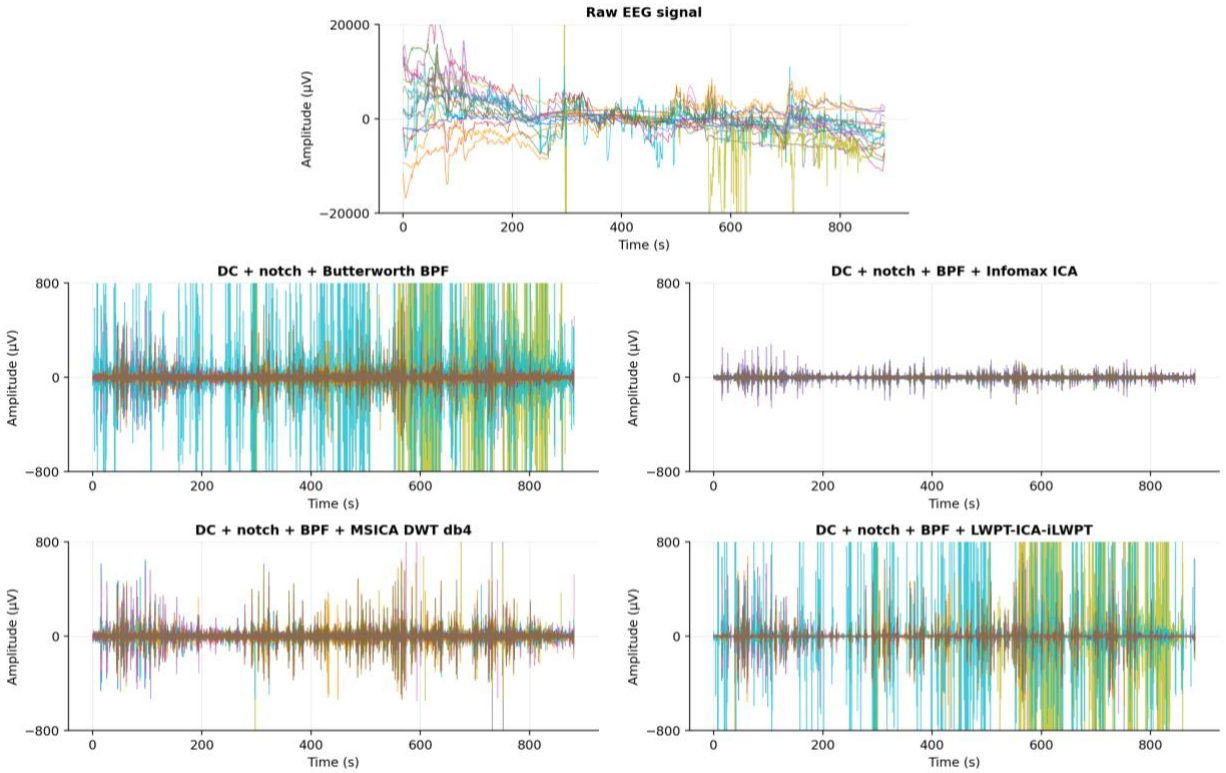

Fig. 2. Comparison of large-amplitude artifact reduction across Infomax ICA, MSICA-DWT, and LWPT-ICA-iLWPT artifact-removal strategies.

convenience-based sampling rather than a formal recruitment protocol. ASD status was confirmed via enrollment at a local special education institution that requires a documented clinical ASD diagnosis for admission; neurotypical participants were recruited from the university community based on proximity and voluntary participation, without a separate clinical screening step to rule out undiagnosed neurodevelopmental conditions. All participants were between 15 and 25 years of age, consistent with the age range reported for the same participant pool by Muliyadi et al. [32]. Studies [30] and [32] used EEG recordings obtained with the same acquisition setup and included participants from the cohort analyzed in the present study; their findings are therefore discussed as related work using overlapping data rather than as independent external validation, and the present comparison with them is contextual rather than a cross-cohort replication. No additional formal inclusion or exclusion criteria (e.g., comorbidity exclusion, medication status, cognitive-level screening) were applied beyond this group assignment, and EEG acquisition personnel were not blinded to participant group during data collection. EEG acquisition was conducted between 09:00 and 12:00 local time; each recording session consisted of a single sitting lasting approximately 15 minutes [30].

B. Preprocessing

For artifact removal, Independent Component Analysis (ICA) remains widely used to attenuate ocular and physiological artifacts [29], [33], [34], [35], [36]. Preprocessing consisted of DC offset removal, notch filtering at 50 Hz and 100 Hz, zero-phase 4th-order Butterworth bandpass filtering from 0.5 to 40 Hz, and Infomax ICA artifact removal. Independent components were flagged as artifactual when ICLabel assigned an artifact-related label (muscle artifact, eye blink, heartbeat, line noise, or channel noise) with probability≥0.50; when no component met this criterion, an EOG-related fallback used Fp1/Fp2 with MNE find_bads_eog threshold 2.0. Two alternative artifact-removal strategies were evaluated for ablation: MSICA-DWT (db4, level 3) [29] and LWPT-ICA-iLWPT (db4-initialized, level 3). These multiscale denoising alternatives, including MSICA-DWT and LWPT-ICA-iLWPT, may provide additional artifact suppression but also introduce further processing stages and tunable parameters; therefore, they were evaluated through the controlled ablation (Section III.D) rather than assuming that one method is universally superior. Fig. 2 shows the resulting reduction in large-amplitude artifacts across the three strategies.

Beyond this qualitative comparison, artifact removal was quantified objectively for every recording by comparing the band-pass signal before and after each artifact-removal stage, channel by channel, and summarizing with the median and interquartile range

Manuscript received 6 July 2026; Revised 4 September 2026; Accepted 15 October 2026; Available online 29 October 2026
Digital Object Identifier (**DOI**): https://doi.org/10.35882/jeeemi.v8i4.1908
Copyright © 2026 by the authors. This work is an open-access article and licensed under a Creative Commons Attribution-ShareAlike 4.0 International License (CC BY-SA 4.0).

(IQR) across channels and subjects (a robust summary is used because a small number of channel reconstructions are numerically unstable; see limitation below). For the Infomax ICA pipeline used in the final model, ICA removed a median of 2 independent components (IQR 1-4) and reduced signal amplitude by a median of 81.9% (IQR 73.6-89.0%), retaining a median of 3.3% (IQR 1.2-7.0%) of the pre-ICA variance, corresponding to a retained-to-removed power ratio of -15.0 dB (IQR -19.5 to -11.1 dB); the large reduction indicates that the excluded components carried the dominant, artifact-related share of the signal energy, while the retained low-amplitude activity reflects cortical EEG. The median waveform correlation between the pre- and post-ICA signals was 0.15 (IQR -0.06-0.27), and the median spectral distortion (1 minus the correlation between pre- and post-ICA power spectra) was 0.042 (IQR 0.020-0.054), indicating that the overall spectral shape was preserved even though most of the raw signal variance, dominated by artifacts, was removed.

C. Windowing

The preprocessed EEG signal was segmented into overlapping windows of 4 seconds with 50% overlap (1000 samples per window, 500-sample hop at 250 Hz); a sensitivity analysis across window lengths $\{2, 4, 8\}$ s and overlap ratios $\{0\%, 25\%, 50\%\}$ yielded an identical subject-level nested-LOSO balanced accuracy of $\mathrm{bAcc} = 0.9375$ across all nine configurations ($\mathrm{AUC} = 0.984$–1.000), indicating that the 4 s/50% setting was not the result of cherry-picking. Because overlapping windows are correlated, this dependence is addressed by design: fold splitting and feature aggregation are performed at the subject level, so correlated windows never cross the train/test boundary, and overlap only enriches the within-subject aggregation statistics rather than introducing additional independent samples. The pooled window-level test set contained 7017 evaluated windows (3575 neurotypical and 3442 ASD); this difference reflects minor natural variation in individual recording duration and does not affect subject-level classification, since window-level features are aggregated into a single fixed-length representation prior to model fitting.

D. WPT Feature Extraction

The Wavelet Packet Transform (WPT) extends conventional wavelet decomposition by decomposing both approximation and detail subbands, thereby providing finer frequency resolution across the analyzed spectrum. WPT decomposition was applied independently to each EEG window using the $\mathrm{sym4}$ mother wavelet at decomposition level 5, producing 32 terminal subbands per channel. The $\mathrm{sym4}$ wavelet was initially selected because it yielded slightly higher window-level accuracy than $\mathrm{db4}$ while maintaining equivalent subject-level balanced accuracy. To ensure that this choice did not introduce selection bias, the wavelet type was subsequently treated as an inner-loop hyperparameter, with the candidate set defined as $\mathcal{W} = \{\mathrm{sym4}, \mathrm{db4}, \mathrm{coif1}, \mathrm{coif2}, \mathrm{sym5}, \mathrm{db6}\}$. Wavelet selection was performed exclusively within the inner leave-one-subject-out (LOSO) loop, ensuring that the outer test subjects did not influence model selection. This procedure produced the same nested-LOSO performance as the fixed-$\mathrm{sym4}$ pipeline, with $\mathrm{bAcc} = 0.9375$ and $\mathrm{AUC} = 1.000$, indicating that the reported performance was not inflated by the initial wavelet choice. At decomposition level $j+1$, node p, the approximation and detail coefficients are computed recursively from level j using the $\mathrm{sym4}$ low-pass filter $h[\cdot]$ and high-pass filter $g[\cdot]$, as given in Eq. (1) and Eq. (2) [37]:

$$A_{j+1,p}[n] = \Sigma_k h[k-2n] \cdot A_{j,p}[k] \quad (1)$$

$$D_{j+1,p}[n] = \Sigma_k g[k-2n] \cdot A_{j,p}[k] \quad (2)$$

where $A_{j,p}(n)$ and $D_{j,p}(n)$ denote the approximation and detail coefficients at decomposition level j and node p, n is the output coefficient index, and k is the input coefficient index of the convolution. For each channel c and terminal node (j,p), the raw subband energy is given in Eq. (3) [37] :

$$E_{raw}(c,j,p) = \Sigma_n \left| W_{c,j,p}[n] \right|^2 \quad (3)$$

where $W_{c,j,p}(n)$ is the n-th WPT coefficient of channel c at node (j,p), and $E_{raw}(c,j,p)$ is the raw energy of that subband. The relative energy feature normalizes E_{raw} by the total energy across all 32 terminal nodes of the same channel [38], as given in Eq. (4) and Eq. (5):

$$E_{total(c)} = \Sigma_{p=0}^{31} E_{raw(c,5,p)} \quad (4)$$

$$E_{rel(c,j,p)} = \frac{E_{raw(c,j,p)}}{E_{total(c)}} \quad (5)$$

where $E_{total}(c)$ is the total energy of channel c summed over the 32 terminal nodes at level $j = 5$. The variance feature at each node is computed from the wavelet coefficients, as given in Eq. (6) and Eq. (7) [38]:

$$\mu(c,j,p) = (1/N) \sum_{(n)} W_{(c,j,p)}[n] \quad (6)$$

$$Var(c,j,p) = (1/N) \sum_{(n)} \left(W_{(c,j,p)}[n] - \mu(c,j,p) \right)^2 \quad (7)$$

where $\mu(c,j,p)$ is the mean of the wavelet coefficients at node (j,p) of channel c, and N denotes the number of coefficients in that node.

The window-level feature vector f concatenates $[E_{rel}(c,j,p), Var(c,j,p)]$ across all 16 channels and 32 subbands, as given in Eq. (8) with the complete

Manuscript received 6 July 2026; Revised 4 September 2026; Accepted 15 October 2026; Available online 29 October 2026
Digital Object Identifier (**DOI**): https://doi.org/10.35882/jeeemi.v8i4.1908
Copyright © 2026 by the authors. This work is an open-access article and licensed under a Creative Commons Attribution-ShareAlike 4.0 International License (CC BY-SA 4.0).

preprocessing and window-level feature-extraction procedure summarized in Algorithm 1:

$$f = [E_{rel}(c,j,p), Var(c,j,p)]_{(c=1,\ldots,16;j=5;p=0,\ldots,31)} \in R^{1024} \quad (8)$$

Algorithm 1. Preprocessing and window-level WPT feature extraction

Input: Raw 16-channel EEG (OpenBCI Cyton board with Daisy module, native 16-channel acquisition) for $N = 16$ subjects; $f_s = 250$ Hz.

Output: Cleaned continuous EEG signal and window-level WPT feature matrix $\boldsymbol{F}$ (1024-dimensional per window) for each subject.

1. For each subject p:
   1.1 Remove DC offset (channel-wise mean).
   1.2 Apply notch filtering at $50/100$ Hz and a zero-phase fourth-order Butterworth bandpass filter over 0.5–40 Hz.
   1.3 Apply Infomax ICA: average-reference; fit ICA (16 components, extended mode, seed $= 42$) on the 1–40 Hz band-passed, clipped signal; flag artifactual components via ICLabel $P_{\text{ICLabel}} \geq 0.5$: muscle/eye/heart/line/channel noise), use an EOG fallback based on Fp1/Fp2 ($r \geq 2.0$) if no components are flagged, and remove the flagged components.
2. For each subject p:
   2.1 Segment the signal into 4 s windows (1000 samples) with 50% overlap (500-sample hop); reject windows with peak-to-peak amplitude $\geq 500\ \mu$V.
   2.2 Apply a five-level WPT using sym4 with periodization to each channel, producing 32 subbands; compute relative energy and variance for each subband.
   2.3 Concatenate the extracted features to form a 1024-dimensional feature vector $\boldsymbol{f}$ for each window.
3. Store $\boldsymbol{F}$, class labels, and subject-group indices for Algorithm 2.

E. Feature Selection and Subject Aggregation

ANOVA F-test SelectKBest was fitted on training-subject windows only, with K selected jointly with C and solver from 20,30,50,100 using the same inner-LOSO grid search described in Section II.F. For feature m, the F-statistic used for ranking [39] is given in Eq. (9):

$$F_m = \frac{\left(\sum_{(g)} \frac{\left(n_g(\overline{(x)}_{(m,g)} - \overline{(x)}_m)^2\right)}{(G-1)}\right)}{\left(\sum_{(g)}\sum_{(i)} \frac{\left((x_{(m,g,i)} - \overline{(x)}_{(m,g)})^2\right)}{(N-G)}\right)} \quad (9)$$

where $G = 2$ is the number of classes, n_g is the number of training windows in class g, N is the total number of training windows, $x_{m,g,i}$ is the value of feature m for the i-th window of class g, $\bar{x}_{m,g}$ is the class-wise mean of feature m, and $\bar{x}_m$ is its overall mean.

For each subject s with W_s windows and K selected features, the four aggregation statistics are given in Eq. (10)-(13) [40] :

$$\mu_k(s) = \frac{(1)}{(W_s)} \sum_{(w=1)}^{(W_s)} f_k\,(s,w) \quad (10)$$

$$\sigma_k(s) = \sqrt{\left(\frac{(1)}{(W_s)} \sum_{(w=1)}^{(W_s)} \left(f_k(s,w) - \mu_k(s)\right)^2\right)} \quad (11)$$

$$m_k(s) = median\{f_k(s,1), \ldots, f_k(s,W_s)\} \quad (12)$$

$$IQR_k(s) = Q_{(0.75,k)}(s) - Q_{(0.25,k)}(s) \quad (13)$$

Algorithm 2. Nested leave-one-subject-out cross-validation with inner hyperparameter selection

Input: Window-level feature matrix $\boldsymbol{F}$ from Algorithm 1; hyperparameter grid $K \in \{20, 30, 50, 100\}$, $C \in \{0.001, 0.01, 0.1, 0.2, 1.0, 10.0\}$, and solver $\in \{\text{liblinear}, \text{lbfgs}\}$.

Output: Pooled subject-level test predictions; selected $(K^*, C^*, \text{solver}^*)$ per outer fold (Table 1).

1. **Outer folds:** In LOSO, each fold holds out one subject as the test subject.
2. **For each outer fold** (training set T, test subject q):
   2.1 **Inner selection:** for each (K, C, solver), perform inner LOSO over T; fit $\text{SelectKBest}(K) + \text{StandardScaler}$ on $T \setminus \{i\}$ only; aggregate using mean, SD, median, and IQR; fit $\text{LR}(C, \text{solver}, \text{balanced})$; and predict subject i.
   2.2 Pool the inner predictions; compute the pooled inner bAcc, AUC, $F1$, and accuracy for each (K, C, solver).
   2.3 Select the configuration $(K^*, C^*, \text{solver}^*)$ with the highest pooled inner bAcc; break ties by higher AUC → F1 → accuracy → fewer convergence warnings → smaller K → smaller C.
   2.4 Refit the selector and scaler on the full training set T; aggregate T; and refit $\text{LR}(C^*, \text{solver}^*)$ on T.
   2.5 Aggregate test subject q using the selector and scaler fitted on T; predict q; and record $(K^*, C^*, \text{solver}^*)$.
3. Pool all outer predictions to obtain the confusion matrix, bAcc, sensitivity, specificity, $F1$, and AUC; report the per-fold hyperparameters, which are available upon request and summarized in

Manuscript received 6 July 2026; Revised 4 September 2026; Accepted 15 October 2026; Available online 29 October 2026
Digital Object Identifier (**DOI**): https://doi.org/10.35882/jeeemi.v8i4.1908
Copyright © 2026 by the authors. This work is an open-access article and licensed under a Creative Commons Attribution-ShareAlike 4.0 International License (CC BY-SA 4.0).

where $f_k(s,w)$ is the value of the k-th selected feature in the w-th window of subject $s (k = 1, \dots, K; w = 1, \dots, W_s)$; $\mu_k(s)$, $\sigma_k(s)$, $m_k(s)$, and $IQR_k(s)$ are its mean, standard deviation, median, and interquartile range across the windows of subject s; and $Q_{0.25,k}(s)$ and $Q_{0.75,k}(s)$ are the first and third quartiles.

The subject-level feature vector $z(s)$ concatenates all four statistics across the K selected features, as given in Eq. (14), with the aggregation procedure detailed within Algorithm 2 [39]:

$$z(s) = [\mu_k(s), \sigma_k(s), m_k(s), IQR_k(s)]_{(k=1)}^{(K)} \in R^{(4K)} \quad (14)$$

F. Classification

Logistic Regression with L2 regularization was used for subject-level classification. Given $z(s)$, weight vector w, and bias b, the linear decision function and predicted ASD probability are given in Eq. (15) and Eq. (16) [40]:

$$\eta(s) = w^T z(s) + b \quad (15)$$

$$P\big(y = 1|z(s)\big) = \frac{(1)}{\Big(1 + exp\big(-\eta(s)\big)\Big)} \quad (16)$$

where $\eta(s)$ is the linear decision score of subject s, the superscript T denotes the transpose, and $y \in \{0,1\}$ is the class label of subject s. The class label is assigned according to the indicator-based threshold rule in Eq. (17) [40] , where $I(\cdot)$ equals 1 if its argument is true and 0 otherwise ($ASD = 1$, $NT = 0$):

$$(\hat{y})(s) = I\big(P\big(y = 1|z(s)\big) \geq 0.5\big) \quad (17)$$

where $\hat{y}(s)$ is the predicted class label of subject s. To mitigate the effect of class imbalance common in small biomedical cohorts [41], the model minimizes an L2-regularized, class-weighted binary cross-entropy objective. The total objective function consists of the positive-class loss, negative-class loss, and L2 regularization term [40], as defined in Eq. (18)–(21), with balanced class weights given in Eq. (22) [41] :

$$\mathcal{L}(w,b) = \mathcal{L}_+(w,b) + \mathcal{L}_-(w,b) + \mathcal{L}_{\text{reg}}(w) \quad (18)$$

$$\mathcal{L}_+(w,b) = -\frac{1}{N}\sum_{s=1}^{N} \alpha_1 \; y(s) \log P\,(s) \quad (19)$$

$$\mathcal{L}_-(w,b) = -\frac{1}{N}\sum_{s=1}^{N} \alpha_0 \big(1 - y(s)\big) \log\big(1 - P(s)\big) \quad (20)$$

$$\mathcal{L}_{\text{reg}}(w) = \frac{1}{2C}\|w\|_2^2 \quad (21)$$

$$\alpha_c = \frac{N}{2N_c},\; c \in \{0,1\} \quad (22)$$

where $\mathcal{L}_+$ and $\mathcal{L}_-$ denote the weighted positive- and negative-class loss terms, respectively; $\mathcal{L}_{\text{reg}}$ denotes the L2 regularization term; $P(s) = P\,\big(y = 1 \mid z(s)\big)$; $y(s)$ is the true class label of subject s; N is the number of training subjects; N_c is the number of training subjects belonging to class c; α_c is the corresponding balanced class weight; and C denotes the inverse regularization strength.

Table 1 summarizes the hyperparameter search space and fixed settings used for model selection and the ablation/statistical comparisons. For each outer LOSO fold, hyperparameter selection was performed using an inner LOSO loop restricted exclusively to the outer-training subjects. Specifically, one subject from the outer-training set was held out as the inner validation subject, while the remaining outer-training subjects were used for model fitting. For each inner fold, the ANOVA SelectKBest step was refit using only the corresponding inner-training subjects. Predictions from all inner folds within a given outer fold were pooled prior to computing the inner balanced accuracy, rather than averaged fold-wise. This procedure was repeated across all outer-training subjects, and the configuration of K, C, and solver with the highest pooled inner balanced accuracy was selected before refitting the model on the full outer-training set; ties were broken by preferring, in order, the higher AUC, the higher $F1$-score, the higher accuracy, fewer solver convergence warnings, and finally the smaller K and smaller C. Across all inner and outer model fits, zero solver convergence warnings were recorded, and the liblinear solver was selected in nearly all folds (15 of 16 nested-LOSO outer folds, with lbfgs selected once); the selected K values ranged from 20 to 50, and the selected C values ranged from 0.001 to 10 across folds. This nested design ensured that the outer test subject never influenced feature selection or hyperparameter tuning. The complete per-fold record of the selected $(K^*, C^*, \text{solver}^*)$ values and inner-loop balanced accuracy for both the nested-LOSO and subject-pair protocols is available from the corresponding author upon reasonable request.

Table 1. Logistic Regression hyperparameter search space and fixed settings.

Parameter	Value
C (regularization strength)	{0.001,0.01,0.1,0.2, 1.0,10.0}
Solver	$\{liblinear, lbfgs\}$
Maximum iterations	1000
Random state	42
Fixed K for ablation/Wilcoxon comparison	$K = 50$
Fixed C for ablation/Wilcoxon comparison	$C = 0.2$
Number of repeated subject-pair evaluations	50 repeats

Manuscript received 6 July 2026; Revised 4 September 2026; Accepted 15 October 2026; Available online 29 October 2026
Digital Object Identifier (**DOI**): https://doi.org/10.35882/jeeemi.v8i4.1908
Copyright © 2026 by the authors. This work is an open-access article and licensed under a Creative Commons Attribution-ShareAlike 4.0 International License (CC BY-SA 4.0).

G. Evaluation Protocol

Model performance was evaluated using accuracy, balanced accuracy (bAcc), sensitivity, specificity, F1-score, and AUC [42]. Balanced accuracy is defined in Eq. (23) [42] :

$$bAcc = \frac{(Sensitivity + Specificity)}{(2)} \quad (23)$$

Sensitivity, specificity, and F1-score are given in Eq. (24)-(26) [42] , where P and R denote Precision and Recall (Sensitivity), respectively, as used in Eq. (26):

$$Sensitivity = \frac{(TP)}{(TP + FN)} \quad (24)$$

$$Specificity = \frac{(TN)}{(TN + FP)} \quad (25)$$

$$F1 = 2 \cdot \frac{(P \cdot R)}{(P + R)} \quad (26)$$

where TP, TN, FP, and FN denote the numbers of true positives, true negatives, false positives, and false negatives, with ASD as the positive class. AUC was computed via the rank-sum (Mann-Whitney U) formulation over the n_1 ASD and n_0 neurotypical subject scores, as given in Eq. (27) [43] :

$$AUC = \frac{\left(\sum R_i - \frac{(n_1(n_1+1))}{(2)}\right)}{(n_1 \cdot n_0)} \quad (27)$$

where R_i is the rank of the i-th ASD subject's predicted probability among all n_1 + n_0 pooled subject scores, and the summation runs over the n_1 ASD subjects. The primary evaluation used nested leave-one-subject-out (LOSO) cross-validation [21], [22], [23], [24]. Although flat (non-nested) cross-validation can be sufficient for algorithm selection in many practical settings with larger datasets [44], the nested design was retained here given the small number of subjects. LOSO was not repeated because the leave-one-subject-out partition is deterministic for a fixed cohort. Repeating LOSO would produce the same test subjects in each fold and would not provide additional independent validation. Therefore, repeated evaluation was applied only to the subject-pair protocol, where ASD-NT pairings can be randomized across repetitions.

Secondary validation used subject-pair cross-validation and repeated subject-pair evaluation (Algorithm 3), with a permutation test assessing whether the observed balanced accuracy exceeded chance level; the 50 repetitions provide the paired basis for the Wilcoxon signed-rank comparison between preprocessing methods (Section III.E). A paired Wilcoxon signed-rank test compared Infomax ICA and MSICA DWT over 50 repeated subject-pair evaluations under a fixed downstream configuration (WPT $sym4$, $K = 50$, Logistic Regression $C = 0.2$). The Wilcoxon test

Algorithm 3. Repeated subject-pair evaluation, cluster-bootstrap confidence interval, and permutation test

Input: Procedure of Algorithm 2 adapted to subject-pair outer folds; repetitions $R = 50$; bootstrap resamples $B = 10{,}000$; permutations T.

Output: $\mathrm{bAcc}/\mathrm{AUC}$ distribution over 50 repetitions; 95% bootstrap CI; permutation p-value.

1. **For** $r = 1, \ldots, 50$**:** seed $= \mathrm{base} + r$; bijective random pairing (8 ASD $\leftrightarrow$ 8 NT, each subject in exactly 1 test pair); for each pair-fold, hold out the pair and run Algorithm 2 Steps 2.1–2.4 on the remaining 14 subjects; pool the 8 pair-folds to obtain bAcc, $F1$, and AUC for repetition r.
2. Report $\mathrm{mean} \pm \mathrm{SD}$ of bAcc and AUC over 50 repetitions.
3. Cluster bootstrap: resample 16 subjects with replacement using stratified sampling, with $B = 10{,}000$; recompute bAcc for each resample; report the 95% percentile CI, which accounts for the non-independence of repetitions.
4. Permutation test: shuffle the subject labels, rerun the full outer CV, and repeat this procedure T times; $p = proportion(shuffledbAcc \geq observed)$.

statistic and matched-pairs effect size are given in Eqs. (28)–(30) [45]:

$$W^+ = \sum_{(i:d_i>0)} rank(|d_i|) \quad (28)$$

$$r = \frac{(Z)}{\left(\sqrt{(N)}\right)} \quad (29)$$

$$d_z = \frac{(\mu_d)}{(\sigma_d)} \quad (30)$$

where d_i is the paired difference in a metric between Infomax ICA and MSICA-DWT in repetition i, $rank(|d_i|)$ is the rank of its absolute value, W^+ is the sum of ranks

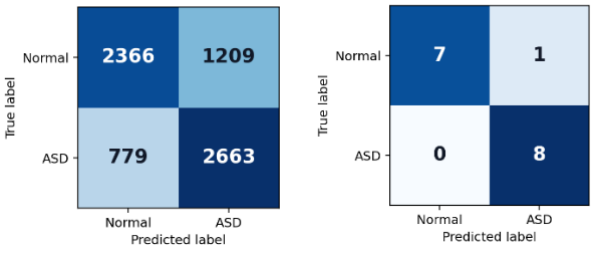

(a) (b)

Fig. 3. Confusion matrices of the proposed method under nested LOSO evaluation: (a) window-level results pooled across all outer test folds and (b) subject-level results after subject-wise aggregation.

Manuscript received 6 July 2026; Revised 4 September 2026; Accepted 15 October 2026; Available online 29 October 2026
Digital Object Identifier (**DOI**): https://doi.org/10.35882/jeeemi.v8i4.1908
Copyright © 2026 by the authors. This work is an open-access article and licensed under a Creative Commons Attribution-ShareAlike 4.0 International License (CC BY-SA 4.0).

of positive differences, Z is the standardized Wilcoxon statistic, $N = 50$ is the number of paired repetitions, and μ_d and σ_d are the mean and standard deviation of the paired differences. Given the small per-class sample size, Wilson score 95% confidence intervals [46] for threshold-based metrics were computed as in Eq. (31):

$$CI_{Wilson} = \frac{\left((\hat{p}) + \frac{(z^2)}{(2n)} \pm z \cdot \sqrt{\left(\frac{\left((\hat{p})(1-(\hat{p})) \right)}{(n)} + \frac{(z^2)}{(4n^2)} \right)} \right)}{\left(1 + \frac{(z^2)}{(n)} \right)} \quad (31)$$

where $\hat{p}$ is the observed proportion (e.g., sensitivity, specificity, or accuracy), n is the number of subjects on which it is computed, and $z = 1.96$ for a 95% interval.

III. Results

A. Main Finding: Subject-Level Performance

Fig. 3 presents the confusion matrices under nested LOSO evaluation. A separate window-level classifier trained on the same subject-wise outer folds achieved only 0.7167 accuracy and 0.7177 balanced accuracy (Fig. 3(a)). In contrast, the proposed Infomax ICA + WPT subject-level aggregation pipeline correctly classified 15 of 16 subjects, achieving 93.75% balanced accuracy, 100% sensitivity, 87.5% specificity, an F1-score of 0.9412, and a nested LOSO AUC of 1.000 (Fig. 3(b)). No ASD subject was misclassified as neurotypical, which is clinically important since false negatives are typically more consequential than false positives in screening contexts. Table 2 provides the corresponding numerical summary of the subject-level classification performance.

Table 2. Main subject-level performance of the proposed framework under nested LOSO and subject-pair cross-validation protocols (Acc = accuracy; bAcc = balanced accuracy).

Protocol	Acc	bAcc	Sens	Spec	F1	AUC
Nested LOSO	0.9375	0.9375	1.000	0.875	0.9412	1.000
Subject-Pair CV	0.9375	0.9375	0.875	1.000	0.9333	0.9688

Given the small per-class sample size ($n = 8$ per group), Wilson score 95% confidence intervals (Eq. (31)) were computed for threshold-based metrics: sensitivity 1.0000 [0.676, 1.000], specificity 0.8750 [0.529, 0.978], and accuracy 0.9375 [0.717, 0.989]. These wide intervals indicate substantial uncertainty despite the favorable point estimates. The substantially lower window-level performance relative to the subject-level result illustrates why subject-level aggregation is necessary for clinically meaningful evaluation.

B. Subject-Level Prediction Scores

Table 3 reports the nested LOSO predicted ASD probability for each subject, directly supporting the $AUC = 1.000$ result. Subject identifiers are anonymized as ASD-01 to ASD-08 and NT-01 to NT-08. Although NT-02 was misclassified as ASD because its probability exceeded the 0.5 threshold (Eq. (17); $P(ASD) = 0.5036$), its score remained lower than every true ASD subject (lowest ASD probability 0.5157), so the rank ordering underlying AUC (Eq. (27)) remained perfect. The reversal of sensitivity and specificity between nested LOSO and subject-pair CV (Table 2) reflects a difference in which held-out pair(s) determined the single misclassification under each protocol, rather than a labeling inconsistency; balanced accuracy remained identical (0.9375) across both designs.

C. Robustness Validation

Repeated subject-pair evaluation was used as a robustness check. Across 50 repeated subject-pair evaluations, the model achieved balanced accuracy of 0.9525 ± 0.0529 and AUC of 0.9897 ± 0.0163. A permutation test confirmed that the observed subject-level performance was unlikely to occur by chance ($p = 0.0196$). The pooled confusion matrix across 50 evaluations yielded 384 TN, 378 TP, 16 FP, and 22 FN out of 800 predictions (pooled accuracy 0.9525, bAcc 0.9525). These counts represent repeated predictions from 16 unique subjects and should not be interpreted as independent observations.

D. Preprocessing Ablation Study

Because the choice of artifact-removal method and feature domain is first applied at the window level before subject-level aggregation, an ablation was conducted to isolate their effect on the final subject-level outcome. Five configurations were evaluated by varying the preprocessing method (Infomax ICA, MSICA DWT, or LWPT-ICA-iLWPT) and the window-level feature domain (WPT relative energy and variance versus non-WPT multidomain features), while keeping the subject-level aggregation and classification pipeline identical across all configurations. Table 4 presents the resulting ablation results under subject-level nested LOSO evaluation. Infomax ICA produced the most stable performance; WPT relative energy and variance features improved

Table 3. Subject-level predicted ASD probabilities under nested LOSO evaluation, grouped by true label (per-subject ID mapping available upon request)

Group	P(ASD) scores ($n = 8$)
ASD	0.5508, 0.5675, 0.5592, 0.5158, 0.7016, 0.9999, 0.5157, 0.5591
NT	0.3921, 0.5036, 0.0217, 0.3295, 0.1925, 0.4717, 0.4242, 0.1790

Manuscript received 6 July 2026; Revised 4 September 2026; Accepted 15 October 2026; Available online 29 October 2026
Digital Object Identifier (**DOI**): https://doi.org/10.35882/jeeemi.v8i4.1908
Copyright © 2026 by the authors. This work is an open-access article and licensed under a Creative Commons Attribution-ShareAlike 4.0 International License (CC BY-SA 4.0).

Table 4. Preprocessing and feature ablation results under subject-level nested LOSO evaluation across five configurations.

Preprocessing	Features	CV	bAcc	AUC
Infomax ICA	WPT rel+var	LOSO	0.9375	1.000
Infomax ICA	non-WPT	LOSO	0.8750	0.9844
MSICA DWT db4	WPT rel+var	LOSO	0.6875	0.7031
MSICA DWT db4	non-WPT	LOSO	0.6250	0.6250
LWPT-ICA-iLWPT	WPT rel+var	LOSO	0.6875	0.6880

performance compared with non-WPT multidomain features under the same subject-level aggregation approach, while MSICA DWT and LWPT-ICA-iLWPT did not improve classification in this strict subject-level setting.

These findings are consistent with the companion study by Rahmat et al. [29] (Introduction), which reported strong pooled window-level performance (up to 99.14% accuracy) using different denoising methods and classifiers on the same cohort; the contrast with the present subject-level results illustrates that window-level and subject-level evaluation can yield different pictures of model performance on the same dataset. The complete preprocessing-ablation and statistical-comparison procedure, including the paired Wilcoxon analysis and robustness checks across classifiers and aggregation schemes, is summarized in Algorithm 4.

Algorithm 4. Preprocessing ablation and statistical comparison

Input: Three preprocessed dataset versions (Infomax ICA, MSICA-DWT, LWPT-ICA-iLWPT); fixed $K = 50$, $C = 0.2$ (no inner-loop tuning, to isolate the preprocessing effect); classifier set {Logistic Regression, linear SVM, RBF SVM, Random Forest, XGBoost} for the robustness check.

Output: Paired Wilcoxon signed-rank statistic and matched-pairs effect size (r, dz) per metric [45]; robustness of the comparison across classifiers and aggregation statistics.

1. For each method m: run 50 repetitions (Algorithm 3, Steps 1) at fixed $K = 50$, $C = 0.2$, identical seeds/folds; record Accuracy/bAcc/F1/AUC/Sensitivity/Specificity per repetition.
2. Per metric: paired Wilcoxon (Infomax ICA vs MSICA-DWT) over 50 repetitions; effect size r, dz.
3. Robustness: repeat Steps 1–2 with classifier ∈ {linear SVM, RBF SVM, Random Forest, XGBoost} and aggregation ∈ {full, mean-only}.

E. Statistical Comparison

Across 50 repeated subject-pair evaluations, Infomax ICA consistently outperformed MSICA DWT across all six metrics (Table 5), with mean differences from +0.16 (Sensitivity) to +0.24 (AUC). All differences were statistically significant ($p = 2.13e-10$ to $4.99e-10$ via Eq. (28)), with maximal matched-pairs effect size ($r = 1.00$, Eq. (29)) and very large standardized effect sizes ($d_z = 2.12 - 4.35$, Eq. (30)). The ceiling value $r \approx 1.00$ reflects complete directional consistency across all 50 repeated evaluations rather than a literally perfect population effect size.

Table 5. Wilcoxon signed-rank statistical comparison between Infomax ICA + WPT and MSICA DWT + WPT across six evaluation metrics.

Metric	Mean diff	p-value	r	dz
Accuracy	+0.1850	2.13e-10	1.00	3.20
bAcc	+0.1850	2.13e-10	1.00	3.20
F1	+0.1804	3.58e-10	1.00	3.26
AUC	+0.2363	3.50e-10	1.00	4.35
Sensitivity	+0.1625	4.99e-10	1.00	2.12
Specificity	+0.2075	3.24e-10	1.00	2.31

Because the 50 repeated evaluations resample pairings from the same 16 subjects rather than drawing 50 independent cohorts, the Wilcoxon result above is best interpreted as a measure of the stability of the Infomax-versus-MSICA-DWT ranking across resampled splits, not as population-level statistical significance. To quantify uncertainty at the level of the original 16 participants, a stratified cluster-bootstrap (resampling subjects with replacement, $B = 10{,}000$) estimated the balanced-accuracy difference between methods: point estimate $+0.187$, 95% CI [0.000, 0.375] ($p \approx 0.066$ by the corresponding bootstrap test), indicating that the participant-level evidence for superiority is directionally consistent but does not reach conventional significance at this cohort size.

IV. Discussion

A. Comparison with Recent EEG-ASD Studies

Table 6 situates the present results relative to recent EEG-based ASD classification studies discussed in Section I, reporting each study's evaluation unit, leakage control, and validation design alongside performance; because these differ substantially, the table serves as contextual reference rather than a like-for-like benchmark. Notably, Shi et al. [17] do not report whether their accuracy reflects the subject or segment level, a distinction that can substantially inflate deep-learning headline accuracies relative to the conservative subject-level nested-LOSO protocol adopted here. Fonseca et al. [47] report a headline accuracy (99.23%) under window-level 10-fold cross-validation without subject-wise splitting, so segments from the same participant may appear in both training and test folds. This configuration may inflate performance estimates relative to the present subject-level protocol. Conversely, Tang et al. [48] report a lower but subject-independent accuracy (85.32% cross-subject on n = 399), consistent with the well-documented drop when the evaluation unit shifts from

Manuscript received 6 July 2026; Revised 4 September 2026; Accepted 15 October 2026; Available online 29 October 2026
Digital Object Identifier (**DOI**): https://doi.org/10.35882/jeeemi.v8i4.1908
Copyright © 2026 by the authors. This work is an open-access article and licensed under a Creative Commons Attribution-ShareAlike 4.0 International License (CC BY-SA 4.0).

Table 6. Contextual comparison with recent EEG-based ASD classification studies differing in cohort, method, and evaluation unit.

Study (Year)	Cohort ASD/NT	Method	Eval. Unit	Dataset Independent (From Ours)	Leakage Control	CI Reported	External Validation	Performance
Ke et al. [13] (2024)	246 / 42	Spectral + coherence, classical ML	Subject	Yes	Partial	Yes	No	AUC = 0.65 [0.54, 0.74]
Rogala et al. [14] (2023)	18/18	Spectral/PLV/ciPLV + LR	Subject (nested CV)	Yes	Yes (nested, 6×5)	No	No	Acc/AUC = 0.83–0.86
Shi et al. [17] (2025)	28/28; 12/5	Deep learning (TFSNet)	Not stated	Yes	Not stated	No	Partial (2 datasets)	Acc = 98.68% / 97.14%
Fonseca et al. [47] (2025)	28 / 28 (Sheffield)	Handcrafted 34-feature + PSO + SVM	Window (2 s, 10-fold)	Yes	No (no subject split)	No	No	Acc = 99.23%
Tang et al. [48] (2024)	280 / 119 (ABC-CT)	Rest-HGCN (graph conv. network), resting-state connectivity	Subject (cross-subject)	Yes	Yes (cross-subject k-fold)	No	No	Acc = 85.32% (cross-subj.); 87.12% (single-subj.)
This study (2026)	8 / 8	WPT + subject aggregation + LR	Subject (nested LOSO)	-	Yes (fold-wise, nested)	Yes	No (acknowledged limitation)	bAcc = 93.75%; AUC = 0.9897 ± 0.0163

window to subject. These differences therefore reflect the evaluation unit and leakage control rather than raw classifier capability. Ke et al. [13], despite a substantially larger cohort (246 ASD, 42 neurotypical) and subject-level evaluation similar in unit to the present protocol, reported a markedly lower AUC of 0.65 [0.54, 0.74]; this contrast likely reflects the trade-off between sample size and cohort homogeneity, as a large multi-site sample introduces clinical and acquisition heterogeneity that a small, tightly controlled single-site cohort such as ours does not. Rogala et al. [14] evaluated a comparably sized cohort (18 ASD, 18 neurotypical) using spectral, PLV, and ciPLV features with Logistic Regression under nested cross-validation, reporting accuracy and AUC in the 0.83–0.86 range; although their design shares the leakage-safe, subject-level spirit of the present protocol, their lower performance may reflect the use of minimally curated clinical EEG recordings rather than the standardized single-site acquisition protocol adopted here.

B. Interpretation and Limitations

The proposed subject-level aggregation framework demonstrated robust performance under strict nested LOSO evaluation. Window-level results (Section III.A) are reported only as a supplementary comparison point, while subject-level performance remains the primary endpoint, particularly because recent methodological studies have shown that segment-wise splitting can inflate EEG classification performance through subject leakage [21], [22], [23]. The nested LOSO AUC of 1.000 warrants explicit interpretation: mathematically, $AUC = 1.000$ (Eq. (27)) occurs on this 16-subject cohort when all 8 ASD probability scores rank above all 8 neurotypical scores, consistent with Fig. 3(b); because the AUC is based on only 64 ASD-control score pairs, it is highly discrete and does not imply generalizability to unseen populations. The repeated subject-pair AUC of 0.9897 ± 0.0163 is therefore the more informative and conservative robustness indicator for comparison against external benchmarks.

The same objective indices used to quantify Infomax ICA (Section II.B) were computed for all three artifact-removal strategies shown in Fig. 2 (Table 7). Only the two scale-invariant indices, waveform correlation and spectral distortion, are directly comparable across methods; artifact-rejection counts use structurally different units (sensor-space components for Infomax ICA, per-subband components for MSICA-DWT, continuous per-subband thresholding for LWPT-ICA-iLWPT), and amplitude change is confounded by output rescaling in MSICA-DWT and LWPT-ICA-iLWPT, so these two descriptors are reported per method only. MSICA-DWT left the signal almost unchanged (correlation 0.998, spectral

Manuscript received 6 July 2026; Revised 4 September 2026; Accepted 15 October 2026; Available online 29 October 2026
Digital Object Identifier (**DOI**): https://doi.org/10.35882/jeeemi.v8i4.1908
Copyright © 2026 by the authors. This work is an open-access article and licensed under a Creative Commons Attribution-ShareAlike 4.0 International License (CC BY-SA 4.0).

Table 7. Objective artifact-removal indices (median [IQR]) across the three compared strategies. Rejection-count and amplitude-change columns are omitted from direct comparison due to differing units and output rescaling (see text)

Preprocessing	Artifact rejection (unit differs)	Correlation before/after	Spectral distortion
Infomax ICA	2 [1–4] sensor-space components	0.15 [-0.06, 0.27]	0.042 [0.020, 0.054]
MSICA-DWT	8 [6–8] per-subband components	0.998 [0.99, 1.00]	0.000 [0.00, 0.00]
LWPT-ICA-iLWPT	Continuous per-subband thresholding	0.59 [0.43, 0.72]	0.015 [0.007, 0.073]

distortion approximately 0), indicating minimal artifact removal, whereas LWPT-ICA-iLWPT produced an intermediate change (correlation 0.59, spectral distortion 0.015). These before/after indices characterize what each method does to the signal rather than establishing which is superior, since no ground-truth clean EEG exists against which to score them; preprocessing superiority is instead attributed to the downstream subject-level classification evidence discussed next.

To assess whether this advantage was an artifact of the specific classifier and aggregation choice, the Infomax-versus-MSICA-DWT comparison was repeated across five classifiers (Logistic Regression, linear SVM, RBF SVM, Random Forest, XGBoost) and two aggregation schemes (full four-statistic aggregation and mean-only). Infomax ICA outperformed MSICA-DWT in all 10 classifier-aggregation combinations, with a mean balanced-accuracy advantage of +0.20 bAcc (range +0.125 to +0.375) and +0.242 AUC, indicating that the advantage is not an artifact of a single downstream configuration; the full per-classifier and per-aggregation breakdown is available from the corresponding author upon reasonable request. This advantage may reflect the small sample size, since multistage denoising can introduce extra parameters that distort distributional features with few subjects; the finding should be read as specific to this cohort and pipeline, and larger datasets may favor more adaptive preprocessing. This distinction between the Wilcoxon comparison (Section III.E, paired across resampled splits) and the participant-level bootstrap CI (Section III.E; 95% CI [0.000, 0.375]) reflects the non-independence already noted in Section III.C: the Wilcoxon result shows the method ranking is stable across resampling, while the bootstrap CI shows this stability does not yet reach conventional significance at the participant level. Both are informative, but only the latter supports population-level inference.

Several limitations should be acknowledged. The cohort size of 16 subjects limits statistical generalizability, and external validation on independent datasets with compatible acquisition parameters was not performed (see Abstract for the corresponding interpretive caveat). All subjects were drawn from a single geographic context, which may limit generalizability across populations. Participants were recruited as two age-band cohorts under the same ethics approval (No. 117/EA/FK/2024) (see Section II.A for recruitment details); individual-level demographic and clinical variables (sex, ASD diagnostic instrument scores, symptom severity, comorbidities, and cognitive level) were not linked to the EEG recordings used in this analysis, and all participants were between 15 and 25 years of age, consistent with the age range reported for the same participant pool by Muliyadi et al. [32]. This limits subgroup-level analysis and formal case-control

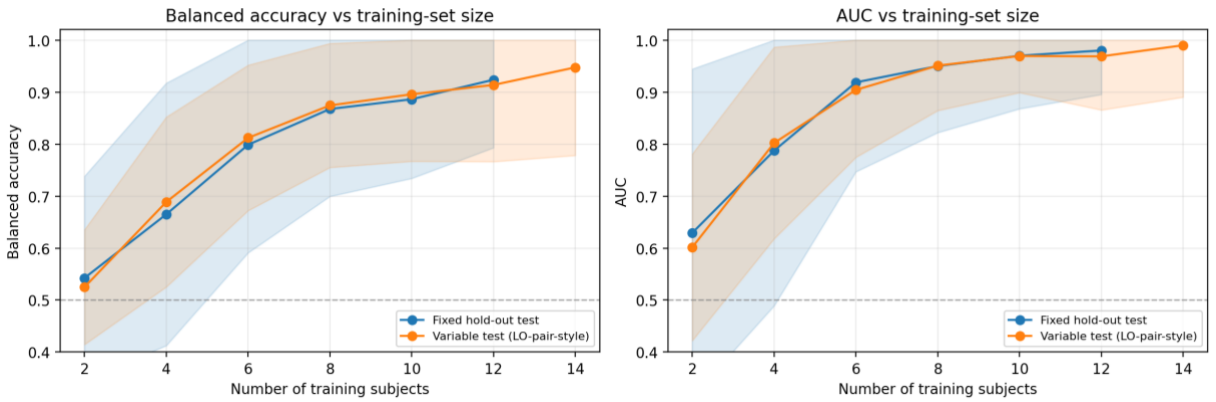

Fig. 4. Subject-level learning curve showing balanced accuracy and AUC as a function of training-set size, under fixed hold-out and variable (leave-pair-style) test designs. Shaded regions indicate variability across resampled training subsets.

Manuscript received 6 July 2026; Revised 4 September 2026; Accepted 15 October 2026; Available online 29 October 2026
Digital Object Identifier (**DOI**): https://doi.org/10.35882/jeeemi.v8i4.1908
Copyright © 2026 by the authors. This work is an open-access article and licensed under a Creative Commons Attribution-ShareAlike 4.0 International License (CC BY-SA 4.0).

matching. In 5 of 256 channel-level reconstructions, occurring in 3 recordings (ASD-04, ASD-06, and NT-07), the post-ICA variance exceeded the pre-ICA variance, which is not physically consistent with pure component removal. This reflects a numerical-stability limitation: sensor-space ICA was fitted with as many components as channels (16) on data that had already been average-referenced, and average referencing reduces the effective rank to 15; requesting a 16th component from rank-15 data can make the whitening/reconstruction ill-conditioned for occasional channels. Because these unstable cases are confined to a small number of channels, the channel-median-based summary reported above is not materially affected by them, which is why robust central tendency (median/IQR) is used throughout rather than the mean. Future implementations should consider a rank-appropriate number of components ($n_{components} = 15$) or a rank-aware ICA formulation; this refinement is not expected to affect the reported classification results, which do not depend on these artifact-quantification indices.

To assess whether performance had plateaued given the small cohort, a learning-curve analysis was conducted by progressively increasing the number of training subjects (Fig. 4). The marginal gain in balanced accuracy decreased from approximately 0.08 per additional subject at small training-set sizes to approximately 0.01-0.02 per subject beyond 8-12 subjects under both fixed and variable test-set designs, indicating that performance is approaching but has not fully reached a plateau at $n = 16$. Future work should evaluate the framework on larger, multicenter cohorts and investigate whether adaptive preprocessing methods become beneficial in higher-data regimes, consistent with recent calls for reproducible, leakage-safe EEG machine learning validation [21], [22], [23], [24].

V. Conclusion

This study developed and validated a subject-level EEG feature-aggregation framework for leakage-safe ASD classification at the individual level. The proposed Infomax ICA + WPT energy-variance framework achieved a nested LOSO balanced accuracy of 93.75%, sensitivity of 100%, specificity of 87.5%, F1-score of 0.9412, and a repeated subject-pair AUC of 0.9897 ± 0.0163 (balanced accuracy 0.9525 ± 0.0529, permutation $p = 0.0196$), with no ASD subject misclassified as neurotypical. A controlled ablation indicated that Infomax ICA outperformed MSICA-DWT under an identical downstream pipeline, but this advantage did not reach statistical significance at the subject level and is reported descriptively. The nested LOSO AUC of 1.000 reflects the discreteness of a 16-subject cohort rather than perfect classification. Compared with deep-learning alternatives, the proposed handcrafted WPT energy-variance pipeline with Logistic Regression offers greater interpretability (per-subband, per-channel features), lower computational cost, and direct alignment with the subject as the clinical unit. These properties are advantageous for small-cohort, resource-constrained screening research, even though deep models may scale better with substantially larger datasets. Future work should extend this framework to larger, multicenter, demographically characterized cohorts to establish external validity, consistent with the directions outlined in Section IV.B.

Acknowledgment

The authors would like to thank Universitas Syiah Kuala, Banda Aceh, Indonesia, for providing facilities and technical support for this study, and sincerely thank all participants who took part in EEG data acquisition.

Declarations

Ethical Approval

This study was approved by the Ethics Clearance Committee under Approval No. 117/EA/FK/2024, in accordance with the 1964 Helsinki Declaration and its later amendments.

Consent to Participate

Written informed consent to participate was obtained from all participants or, where applicable, from their parents or legal guardians before data collection.

Consent for Publication

Consent for publication of anonymized and aggregated study findings was obtained from all participants or, where applicable, from their parents or legal guardians.

Funding

This research received no specific grant from any funding agency in the public, commercial, or not-for-profit sectors.

Competing Interests

The authors declare that they have no competing interests.

Data Availability

The data supporting the findings of this study are not publicly available due to ethical restrictions and participant privacy but may be made available from the corresponding author upon reasonable request and subject to institutional ethics approval.

Author Contributions

Zaky Naufal: conceptualization, EEG feature-extraction methodology, software, formal analysis, drafting,

Manuscript received 6 July 2026; Revised 4 September 2026; Accepted 15 October 2026; Available online 29 October 2026
Digital Object Identifier (**DOI**): https://doi.org/10.35882/jeeemi.v8i4.1908
Copyright © 2026 by the authors. This work is an open-access article and licensed under a Creative Commons Attribution-ShareAlike 4.0 International License (CC BY-SA 4.0).

visualization. Melinda Melinda: conceptualization, methodology, supervision, project administration, funding acquisition, review. Siti Rusdiana: methodological development, validation of the analysis pipeline, formal analysis, review. Yunidar Yunidar: methodological development, validation, data investigation, resources, data curation, supervision, review. Aufa Rafiki: validation, visualization, review. Lola Vivita: resources, project administration, review. All authors reviewed and approved the final manuscript and agreed to be accountable for all aspects of the work.

Generative AI and AI-Assisted Technologies

The authors declare that generative AI and AI-assisted technologies were not used to generate scientific results, perform data analysis, interpret findings, or formulate scientific conclusions. If AI-assisted tools were used for language editing or proofreading, their use was limited to improving readability and language quality, and all outputs were reviewed and verified by the authors, who take full responsibility for the manuscript.

References

[1] C. J. L. Murray and GBD 2021 Collaborators, "Findings from the Global Burden of Disease Study 2021," *Lancet*, vol. 403, no. 10440, pp. 2259–2262, May 2024, doi: 10.1016/S0140-6736(24)00769-4.

[2] J. Li *et al.*, "Identification of autism spectrum disorder based on electroencephalography: A systematic review," *Comput. Biol. Med.*, vol. 170, Art. no. 108075, Mar. 2024, doi: 10.1016/j.compbiomed.2024.108075.

[3] S. Das et al., "Machine learning approaches for electroencephalography and magnetoencephalography analyses in autism spectrum disorder: A systematic review," Prog. Neuropsychopharmacol. Biol. Psychiatry, vol. 123, Art. no. 110705, Apr. 2023, doi: 10.1016/j.pnpbp.2022.110705.

[4] S. J. Webb et al., "The Autism Biomarkers Consortium for Clinical Trials: Initial evaluation of a battery of candidate EEG biomarkers," Am. J. Psychiatry, vol. 180, no. 1, pp. 41–49, Jan. 2023, doi: 10.1176/appi.ajp.21050485.

[5] X. Geng et al., "Abnormalities of EEG functional connectivity and effective connectivity in children with autism spectrum disorder," Brain Sci., vol. 13, no. 1, Art. no. 130, Jan. 2023, doi: 10.3390/brainsci13010130.

[6] S. Kurkin et al., "Features of the resting-state functional brain network of children with autism spectrum disorder: EEG source-level analysis," Eur. Phys. J. Spec. Top., vol. 232, no. 5, pp. 683–693, 2023, doi: 10.1140/epjs/s11734-022-00717-0.

[7] M. Milovanovic and R. Grujicic, "Electroencephalography in assessment of autism spectrum disorders: A review," Front. Psychiatry, vol. 12, Art. no. 686021, Sep. 2021, doi: 10.3389/fpsyt.2021.686021.

[8] J. Shan et al., "A scoping review of physiological biomarkers in autism," Front. Neurosci., vol. 17, Art. no. 1269880, Sep. 2023, doi: 10.3389/fnins.2023.1269880.

[9] B. Sun et al., "Identification of diagnostic markers for ASD: A restrictive interest analysis based on EEG combined with eye tracking," Front. Neurosci., vol. 17, Art. no. 1236637, Oct. 2023, doi: 10.3389/fnins.2023.1236637.

[10] B. Sun et al., "Interest paradigm for early identification of autism spectrum disorder: An analysis from electroencephalography combined with eye tracking," Front. Neurosci., vol. 18, Art. no. 1502045, Nov. 2024, doi: 10.3389/fnins.2024.1502045.

[11] L. Bogéa Ribeiro and M. da Silva Filho, "Systematic review on EEG analysis to diagnose and treat autism by evaluating functional connectivity and spectral power," Neuropsychiatr. Dis. Treat., vol. 19, pp. 415–424, 2023, doi: 10.2147/NDT.S394363.

[12] P. Garcés et al., "Resting state EEG power spectrum and functional connectivity in autism: A cross-sectional analysis," Mol. Autism, vol. 13, no. 1, Art. no. 22, May 2022, doi: 10.1186/s13229-022-00500-X.

[13] S. Y. Ke et al., "Classification of autism spectrum disorder using electroencephalography in Chinese children: A cross-sectional retrospective study," Front. Neurosci., vol. 18, Art. no. 1330556, Jan. 2024, doi: 10.3389/fnins.2024.1330556.

[14] J. Rogala et al., "Enhancing autism spectrum disorder classification in children through the integration of traditional statistics and classical machine learning techniques in EEG analysis," Sci. Rep., vol. 13, no. 1, Art. no. 21748, Dec. 2023, doi: 10.1038/s41598-023-49048-7.

[15] Y. Xu, Z. Yu, Y. Li, Y. Liu, Y. Li, and Y. Wang, "Autism spectrum disorder diagnosis with EEG signals using time series maps of brain functional connectivity and a combined CNN–LSTM model," Comput. Methods Programs Biomed., vol. 250, Art. no. 108196, Jun. 2024, doi: 10.1016/j.cmpb.2024.108196.

[16] N. K. Al-Qazzaz, A. A. Aldoori, A. K. Buniya, S. H. B. M. Ali, and S. A. Ahmad, "Transfer learning and hybrid deep convolutional neural networks models for autism spectrum disorder classification from EEG signals," IEEE Access, vol. 12, pp. 64510–

Manuscript received 6 July 2026; Revised 4 September 2026; Accepted 15 October 2026; Available online 29 October 2026
Digital Object Identifier (**DOI**): https://doi.org/10.35882/jeeemi.v8i4.1908
Copyright © 2026 by the authors. This work is an open-access article and licensed under a Creative Commons Attribution-ShareAlike 4.0 International License (CC BY-SA 4.0).

64530, 2024, doi: 10.1109/ACCESS.2024.3396869.
[17] L. Shi et al., "TFSNet: A time–frequency synergy network based on EEG signals for autism spectrum disorder classification," Brain Sci., vol. 15, no. 7, Art. no. 684, Jun. 2025, doi: 10.3390/brainsci15070684.
[18] W. Hu, G. Jiang, J. Han, X. Li, and P. Xie, "Regional-asymmetric adaptive graph convolutional neural network for diagnosis of autism in children with resting-state EEG," IEEE Trans. Neural Syst. Rehabil. Eng., vol. 32, pp. 200–211, 2024, doi: 10.1109/TNSRE.2023.3347134.
[19] P. Chawla, S. B. Rana, H. Kaur, and K. Singh, "Computer-aided diagnosis of autism spectrum disorder from EEG signals using deep learning with FAWT and multiscale permutation entropy features," Proc. Inst. Mech. Eng. H, vol. 237, no. 2, pp. 282–294, Feb. 2023, doi: 10.1177/09544119221141751.
[20] G. Eroğlu, "Electroencephalography-based machine learning for biomarker detection in dyslexia and autism spectrum disorder: A comparative review of models, features, and diagnostic utility," Diagnostics, vol. 15, no. 18, Art. no. 2388, Sep. 2025, doi: 10.3390/diagnostics15182388.
[21] S. Kapoor and A. Narayanan, "Leakage and the reproducibility crisis in machine-learning-based science," Patterns, vol. 4, no. 9, Art. no. 100804, Sep. 2023, doi: 10.1016/j.patter.2023.100804.
[22] G. Brookshire et al., "Data leakage in deep learning studies of translational EEG," Front. Neurosci., vol. 18, Art. no. 1373515, May 2024, doi: 10.3389/fnins.2024.1373515.
[23] F. Del Pup, A. Zanola, L. F. Tshimanga, A. Bertoldo, L. Finos, and M. Atzori, "The role of data partitioning on the performance of EEG-based deep learning models in supervised cross-subject analysis: A preliminary study," Comput. Biol. Med., vol. 196, Art. no. 110608, Sep. 2025, doi: 10.1016/j.compbiomed.2025.110608.
[24] T. J. Bradshaw, Z. Huemann, J. Hu, and A. Rahmim, "A guide to cross-validation for artificial intelligence in medical imaging," Radiol. Artif. Intell., vol. 5, no. 4, Art. no. e220232, Jul. 2023, doi: 10.1148/ryai.220232.
[25] S. Luo, P. Ren, J. Wu, X. Wu, and X. Zhang, "Feature extraction method of EEG based on wavelet packet reconstruction and deep learning model of VR motion sickness feature classification and prediction," PLoS One, vol. 19, no. 7, Art. no. e0305733, Jul. 2024, doi: 10.1371/journal.pone.0305733.
[26] Q. M. Ud Din and A. K. Jayanthy, "Wavelet scattering transform and deep learning networks based autism spectrum disorder identification using EEG signals," Traitement du Signal, vol. 39, no. 6, pp. 2069–2076, Dec. 2022, doi: 10.18280/TS.390619.
[27] H. Albaqami, G. M. Hassan, A. Subasi, and A. Datta, "Automatic detection of abnormal EEG signals using wavelet feature extraction and gradient boosting decision tree," Biomed. Signal Process. Control, vol. 70, Art. no. 102957, Sep. 2021, doi: 10.1016/j.bspc.2021.102957.
[28] Y. Wang, C. Song, T. Zhang, Z. Yao, Z. Chang, and D. Wang, "Feature extraction of motor imagery EEG via discrete wavelet transform and generalized maximum fuzzy membership difference entropy: A comparative study," Electronics, vol. 12, no. 10, Art. no. 2207, May 2023, doi: 10.3390/electronics12102207.
[29] M. M. Rahmat, Y. Yunidar, and M. Melinda, "A comparative study of MSPCA and MSICA denoising for EEG based autism spectrum disorder classification using LightGBM and TCN-SA," Int. J. Intell. Eng. Syst., vol. 19, no. 6, pp. 186–201, Jun. 2026, doi: 10.22266/ijies2026.0630.11.
[30] M. Muliyadi, M. Melinda, Y. Away, S. Gazali, A. Rafiki, and W. K. Wong, "Bayesian-optimized Butterworth-PID preprocessing for EEG-based autism spectrum disorder classification," IEEE Access, vol. 14, pp. 100364–100382, 2026, doi: 10.1109/ACCESS.2026.3709120.
[31] J. Sabio, N. S. Williams, G. M. McArthur, and N. A. Badcock, "A scoping review on the use of consumer-grade EEG devices for research," PLoS One, vol. 19, no. 3, Art. no. e0291186, Mar. 2024, doi: 10.1371/journal.pone.0291186.
[32] M. Muliyadi, M. Melinda, Y. Away, S. Gazali, A. Rafiki, and W. K. Wong, "Temporal deep learning with multiscale principal component features for autism classification from electroencephalographic signals," Journal of Electronics, Electromedical Engineering, and Medical Informatics, vol. 8, no. 3, pp. 1239–1259, Jul. 2026, doi: 10.35882/jeeemi.v8i3.1735.
[33] Z. Jamil, A. Jamil, and M. Majid, "Artifact removal from EEG signals recorded in non-restricted environment," Biocybern. Biomed. Eng., vol. 41, no. 2, pp. 503–515, Apr. 2021, doi: 10.1016/j.bbe.2021.03.009.
[34] P. Arpaia et al., "A systematic review of techniques for artifact detection and artifact category identification in electroencephalography from wearable devices," Sensors, vol. 25, no. 18, Art. no. 5770, Sep. 2025, doi: 10.3390/s25185770.
[35] S. S. Khan, J. S. Sudan, A. Pathak, R. Pandit, P. Rane, and A. K. Kumawat, "A review of EEG artifact removal methods for brain-computer interface applications," Ingénierie des Systèmes

Manuscript received 6 July 2026; Revised 4 September 2026; Accepted 15 October 2026; Available online 29 October 2026
Digital Object Identifier (**DOI**): https://doi.org/10.35882/jeeemi.v8i4.1908
Copyright © 2026 by the authors. This work is an open-access article and licensed under a Creative Commons Attribution-ShareAlike 4.0 International License (CC BY-SA 4.0).

d'Information, vol. 29, no. 1, pp. 247–252, Feb. 2024, doi: 10.18280/ISI.290124.
[36] A. Chaddad, Y. Wu, R. Kateb, and A. Bouridane, "Electroencephalography signal processing: A comprehensive review and analysis of methods and techniques," Sensors, vol. 23, no. 14, Art. no. 6434, Jul. 2023, doi: 10.3390/s23146434.
[37] R. R. Coifman and M. V. Wickerhauser, "Entropy-based algorithms for best basis selection," IEEE Trans. Inf. Theory, vol. 38, no. 2, pp. 713–718, 1992, doi: 10.1109/18.119732.
[38] O. A. Rosso et al., "Wavelet entropy: A new tool for analysis of short duration brain electrical signals," J. Neurosci. Methods, vol. 105, no. 1, pp. 65–75, Jan. 2001, doi: 10.1016/S0165-0270(00)00356-3.
[39] I. Guyon and A. Elisseeff, "An introduction to variable and feature selection," J. Mach. Learn. Res., vol. 3, pp. 1157–1182, Mar. 2003. [Online]. Available: https://www.jmlr.org/papers/v3/guyon03a.html
[40] T. Hastie, R. Tibshirani, and J. Friedman, The Elements of Statistical Learning: Data Mining, Inference, and Prediction, 2nd ed. New York, NY, USA: Springer, 2009, doi: 10.1007/978-0-387-84858-7.
[41] M. Salmi, D. Atif, D. Oliva, A. Abraham, and S. Ventura, "Handling imbalanced medical datasets: Review of a decade of research," Artif. Intell. Rev., vol. 57, no. 10, Art. no. 273, Sep. 2024, doi: 10.1007/s10462-024-10884-2.
[42] T. Fawcett, "An introduction to ROC analysis," Pattern Recognit. Lett., vol. 27, no. 8, pp. 861–874, Jun. 2006, doi: 10.1016/j.patrec.2005.10.010.
[43] J. A. Hanley and B. J. McNeil, "The meaning and use of the area under a receiver operating characteristic (ROC) curve," Radiology, vol. 143, no. 1, pp. 29–36, 1982, doi: 10.1148/radiology.143.1.7063747.
[44] J. Wainer and G. Cawley, "Nested cross-validation when selecting classifiers is overzealous for most practical applications," Expert Syst. Appl., vol. 182, Art. no. 115222, Nov. 2021, doi: 10.1016/j.eswa.2021.115222.
[45] C. O. Fritz, P. E. Morris, and J. J. Richler, "Effect size estimates: Current use, calculations, and interpretation," J. Exp. Psychol. Gen., vol. 141, no. 1, pp. 2–18, 2012, doi: 10.1037/a0024338.
[46] L. D. Brown, T. T. Cai, and A. DasGupta, "Interval estimation for a binomial proportion," Stat. Sci., vol. 16, no. 2, pp. 101–133, May 2001, doi: 10.1214/ss/1009213286.
[47] F. S. Fonseca et al., "Supporting ASD diagnosis with EEG, ML and swarm intelligence: Early detection of autism spectrum disorder based on electroencephalography analysis by machine learning and swarm intelligence," AI Sens., vol. 1, no. 1, Art. no. 3, Jun. 2025, doi: 10.3390/aisens1010003.
[48] T. Tang et al., "A hybrid graph network model for ASD diagnosis based on resting-state EEG signals," Brain Res. Bull., vol. 206, Art. no. 110826, Jan. 2024, doi: 10.1016/j.brainresbull.2023.110826.

Author Biography

Zaky Naufal was born in Banda Aceh, Indonesia, on March 19, 1998. He received his Bachelor's degree in 2021 from the Department of Electrical and Computer Engineering, Faculty of Engineering, Universitas Syiah Kuala, where he focus his undergraduate work on signal processing. He is currently pursuing a Master's degree in Electrical Engineering at the same institution, with research centered on electroencephalography (EEG) signal processing, wavelet-based feature extraction, and machine learning for autism spectrum disorder classification. Alongside his graduate studies, he works as a Manggala Informatika Ahli Pertama (functional informatics officer) at the Communications, Informatics, and Cryptography Office (Diskominsa) of Aceh Province, an experience that has broadened his interest in applied information systems and data-driven governance. His research interests span biomedical signal processing and machine learning for neurodevelopmental disorder classification. He can be contacted at zaky.24@mhs.usk.ac.id.

Melinda was born in Bireuen, Aceh, on June 10, 1979. She received a B.Eng degree from the Department of Electrical and Computer Engineering, Faculty of Engineering, Universitas Syiah Kuala, Banda Aceh, in 2002. She completed her master's degree at the Faculty of Electrical Department, University of Southampton, United Kingdom, with a concentration in field study of Radio Frequency Communication Systems in 2009. She completed her Doctoral degree at the Department of Electrical Engineering, Faculty of Engineering, Universitas Indonesia, in February 2018. She has been with the Department of Electrical Engineering, Faculty of Engineering, Universitas Syiah Kuala since 2002. Her research interests include multimedia signal processing and fluctuation processing. She can be contacted at email: melinda@usk.ac.id.

Manuscript received 6 July 2026; Revised 4 September 2026; Accepted 15 October 2026; Available online 29 October 2026
Digital Object Identifier (**DOI**): https://doi.org/10.35882/jeeemi.v8i4.1908
Copyright © 2026 by the authors. This work is an open-access article and licensed under a Creative Commons Attribution-ShareAlike 4.0 International License (CC BY-SA 4.0).

Siti Rusdiana was born in Banda Aceh, Indonesia, on 10 September 1963. She received the B.S. degree in mathematics science from Institut Teknologi Sepuluh Nopember, Surabaya, Indonesia, in 1988, the M.Eng. degree in mathematics science from Osaka University, Osaka, Japan, in 1998, and the Ph.D. degree in applied mathematics from Universitas Sumatera Utara, Medan, Indonesia, in 2013. She was the Chairperson of the Department of Mathematics, Universitas Syiah Kuala, Banda Aceh, Indonesia (1998 – 2004). From 2013 to 2020, she was the Head of the Laboratory for Dynamic and Optimization Applications, Department of Mathematics, Universitas Syiah Kuala, where she has been an Associate Professor in the Department of Mathematics since 2014. She is also a member of IEEE. Her research interests in applied mathematics include optimization, operations research, and data science. She can be contacted at email: siti.rusdiana@usk.ac.id.

Yunidar was born in Banda Aceh, Aceh, on June 29th, 1974. She has been a lecturer at the Faculty of Engineering, Department of Electrical and Computer Engineering, Universitas Syiah Kuala, since March 2000. After completing her undergraduate education in Physics at Universitas Syiah Kuala, Aceh Indonesia, in 1997, she then obtained a master of engineering (MT) degree in Optoelectrotechnics and Laser Applications from the University of Indonesia, Jakarta Indonesia, in 2000. After which, she took a doctoral degree program in electrical and computer engineering at Syiah Kuala University and graduated in 2025. She is also a member of IEEE. Her research interests include the implementation of biomedical engineering and sensors used in biomedical applications, including multimedia. She can be contacted at email: yunidar@usk.ac.id.

Aufa Rafiki was born on April 20, 2003, in Banda Aceh, Indonesia. He received the Bachelor of Computer Engineering degree from Universitas Syiah Kuala in Banda Aceh, Indonesia, in 2025. He received the Master of Electrical Engineering degree, with a concentration in Biomedical Engineering, from Universitas Syiah Kuala through a fast-track program. He has been involved in several research projects related to EEG signal processing, artificial intelligence, deep learning, and technology-assisted early detection of autism spectrum disorder. His research interests include biomedical signal processing, EEG analysis, artificial intelligence, machine learning, deep learning, and medical technology for autism spectrum disorder detection. He can be contacted at email: aufa35@mhs.usk.ac.id.

Lola Vivita was born in Malang, East Java, Indonesia, on October 29, 1978. She received a Basic Engineering Degree from the Department of Architecture Engineering, Faculty of Engineering, Universitas Syiah Kuala, Banda Aceh in 2002. She completed her master's degree at the Faculty of Civil Department, Universitas Syiah Kuala, Banda Aceh with a concentration in field study of Urban Infrastructure Management in 2010. She has already completed her Doctoral degree at the Department of Doctoral Engineering Science, Faculty of Engineering, Universitas Syiah Kuala, Banda Aceh in November 2023. She has been with the Banda Aceh City Government since April 2005. Her research interests include architecture and disaster mitigation. She can be contacted at email: lola.vivita1978@gmail.com.

Manuscript received 6 July 2026; Revised 4 September 2026; Accepted 15 October 2026; Available online 29 October 2026
Digital Object Identifier (**DOI**): https://doi.org/10.35882/jeeemi.v8i4.1908
Copyright © 2026 by the authors. This work is an open-access article and licensed under a Creative Commons Attribution-ShareAlike 4.0 International License (CC BY-SA 4.0).